Manon Farvacque · Christophe Corona · Jérôme Lopez-Saez · Robin Mainieri ·
Markus Stoffel · Franck Bourrier · Nicolas Eckert · David Toe

# Estimating rockfall release frequency from blocks deposited in protection barriers, growth disturbances in trees, and trajectory simulations

**Abstract** The spatial and temporal quantification of rockfall frequency remains a major challenge in mountain environments, especially also in terms of rockfall management. Approaches that have been used traditionally to quantify rockfall frequency include historical records, remote sensing, or *in situ* monitoring, but have been shown repeatedly to suffer from a lack of completeness or to rely on rather short time series (of a few years) that are, in addition, limited to small areas. As such, they normally cannot meet the stringent requirements of hazard and risk analyses. Here, we propose a new procedure coupling field analysis of rockfall deposits in mitigation structures and growth disturbances in tree-ring series with three-dimensional (3D), process-based rockfall modeling to estimate rockfall frequencies for individual cliff compartments. This procedure has been tested on a slope in the Swiss Alps (La Fory, Sembrancher VS), where rockfall triggered from a 38 hm$^2$ cliff to threaten a 1-km-long section of the road to the Grand St. Bernard tunnel and the local railway line. Based on 84 rockfall deposits retrieved from 420-m-long protection barrier and growth disturbances in trees over the 1994–2017 period, we estimate rockfall hazard to between 0.043 and 0.348 events yr$^{-1}$ at various locations on the slope. In total, we used 68,680,000 rockfall simulations to translate hazard values into rockfall frequencies at the cliff level. Converging release frequencies between tree-ring analyses (0.99–1.35 events yr$^{-1}$ hm$^{-2}$) and values obtained from deposits in the protection barrier (0.82 events yr$^{-1}$ hm$^{-2}$) confirm the reliability of our procedure. Despite remaining limitations, our approach enables precise quantification of rockfall release frequency in a holistic and reproducible manner both in space (a few hm$^2$) and time (several decades), and thus yields the data needed for hazard and risk mapping. We therefore recommend, where applicable, to include this procedure in future rockfall management strategies.

**Keywords** Release frequency · Block deposits · Protection barriers · Dendrogeomorphology · Trajectory simulations · Swiss Alps

## Introduction

Rockfall events are a common type of fast moving landslide (Hungr et al. 2014), described as the detachment of individual rocks of any size from (sub)vertical outcrops followed by rapid to extremely rapid downslope motions characterized by free falling, bouncing and/or rolling (Lambert 2011; Ferrari et al. 2016). Rockfall is a major and chronic hazard in mountain areas, endangering human lives, transportation infrastructure, industries and residences— and more generally the areas beneath cliffs (Benjamin et al. 2020). Even if rockfall does not pose the same level of economic risk as large-scale landslides, the process is indeed responsible for a similar number of accidents and fatalities (Ferrari et al. 2016). As a consequence, rockfall risk assessment is of major interest to public authorities, stakeholders and civil protection officers (Crosta and Agliardi 2003; Volkwein et al. 2011; Wang et al. 2014). To satisfy the needs of risk managers (Dussauge-Peisser et al. 2002), prioritization of mitigation actions, countermeasure selection, and land-use planning must be supported by quantitative and spatially distributed rockfall hazard modeling procedures (Volkwein et al. 2011) in which the frequency and magnitude of rockfall events are of paramount importance as they control the dynamics (trajectory, velocity, energy, runout distances) of falling masses, and thus, their interactions with and impacts on elements at risk (Giani et al. 2004; Bourrier and Hungr 2013; Asteriou et al. 2013).

Over the last decades, rockfall propagation has been studied extensively and several models have been developed to reliably simulate the trajectories, runout distances and kinetic energy of blocks (Stevens 1998; Agliardi and Crosta 2003; Bourrier et al. 2009; Volkwein et al. 2011; Dorren 2012; Budetta et al. 2016). In terms of rockfall frequency, remotely sensed data derived from photogrammetry (Budetta et al. 2016; Matasci et al. 2018), remote-sensing tools (Ferrero et al. 2016; Umili et al. 2020) or LiDAR (Strunden et al. 2015; Macciotta et al. 2015; D'Amato et al. 2016; Matasci et al. 2018), as well as seismic and infrasound sensors (Zimmer and Sitar 2015; Feng et al. 2020) have vastly improved rockfall detection, thus enabling a more accurate estimation of rockfall release frequency at the cliff level. However, as these approaches have been applied to rockfall cliffs only fairly recently, they cover only relatively short time periods (a few years at best) and thus may not capture the full breadth of the sometimes sporadic nature of rockfall activity (Guerin et al. 2020). In addition, given their cost and limited flexibility, these monitoring approaches remain restricted to small cliff faces most of the time.

Long-term and large-scale records of rockfall activity are provided by alternative approaches, such as historical inventories (Dussauge et al. 2003; Eckert et al. 2020), optically stimulated luminescence (OSL; Kanari et al. 2019), or terrestrial cosmogenic nuclide (TCN; Gallach et al. 2018) approaches, for either a specific cliff or larger regions (Guerin et al. 2020). Yet, rockfall inventories remain scarce (Ferrero et al. 2016) and continue to suffer from biases related to non-observed

events (Volkwein et al. 2011; Guerin et al. 2020), whereas OSL and TCN approaches are time-consuming and provide estimations of past rockfall occurrence covering several millennia—and may not necessarily be representative of present-day activity. In addition, the latter approaches are mainly focused on extreme events and only partially reflect the full breadth of rockfall activity at the cliff level.

As a consequence, in view of the above-mentioned limitations, the quantification of onset probability at the cliff scale and for periods spanning decades to centuries remains a major limitation in most rockfall hazard assessments (Dussauge-Peisser et al. 2002). Here, in order to fill this knowledge gap, we propose a new method to estimate rockfall release frequency for large cliff compartments by coupling field-based data from rockfall protection barriers and tree-ring records of past rockfall activity with three-dimensional (3D), process based rockfall modeling approaches. Our approach has been developed at La Fory (Sembrancher, Swiss Alps) where numerous rockfalls have been reported by local authorities. At the site, we estimated rockfall hazard over the last decades, at different elevations along the slope from rockfall deposits in protection barriers and growth disturbances found in tree-ring records. In a second step, we combined these records with a rockfall model to reconstruct the number of rockfall releases in space and time (release frequency) over a 38 hm$^2$ cliff threatening >1 km of transport infrastructure networks (road, railway) on the valley floor. The approach presented here is reproducible on a wide range forested slopes where historical archives are largely missing, and therefore offers risk practitioners a valuable alternative to high quality, yet expensive and sophisticated approaches that are constrained both temporally (surveys rarely exceed a few years) or spatially (monitoring is most of the time restricted to small-scale sites).

### Proposed methodology

In rockfall terminology, hazard refers to the probability of an event (rockfall) to occur over a predefined period of time and within a given area (Varnes 1984; Ferrari et al. 2016). In this study, we express rockfall hazard $H_z$ at a given location $z$ as:

$$H_z = f \times p_z \tag{1}$$

where $f$ (expressed as the number of events per year) is the frequency of a rockfall release from a given, unstable source over a given time interval, and $p_z$ is the probability (ranging between 0-1) that a falling rock will propagate down to a location $z$.

Assuming that the failure process is homogeneously distributed across the unstable source, the rockfall frequency $f$ can be expressed as:

$$f = S \times \lambda \tag{2}$$

where $S$ is the surface of the rockfall source, and $\lambda$ the number of rocks falling from that surface per unit of surface and time.

Based on Eqs. (1) and (2), the release frequency $\lambda$ can thus be considered as:

$$\lambda = \frac{H_z}{S \times p_z} \tag{3}$$

Following Eq. (3), we quantify here rockfall release frequency $\lambda$ with a two-step procedure: in a first step, we evaluate $H$ at different locations $z$, i.e., at the level of protection barriers and on the basis of injured trees, using the number of rocks deposited in mitigation structures and growth disturbances in tree-ring series, respectively. In a second step, we use rockfall numerical modeling to quantify the probability that blocks falling from cliff $S$ propagate down to location $z$. Figure 1 shows the general scheme of the framework used in this paper to assess rockfall release frequency. We implement our methodology at La Fory slope where (1) rockfall is the dominant process and (2) damaged trees as well as mitigation structures allow quantification of rockfall hazard over the last decades.

## Application

### Study site

The study site, known as *La Fory* (46°05'02"N, 07°06'48"E), is situated in the Canton of Valais (Swiss Alps), on the territory of Sembrancher (Fig. 2A, B). The area under investigation covers 0.3 km$^2$ from the summit of *Le Troubayet* (1325 m asl) to the *Dranse* River (641 m asl; Fig. 2C). Slope angles range from 67° in the upper section of the study site to 6° next to the river, with a mean of ~37° across the slope. The site is characterized by abrupt cliffs (Fig. 2C, D) consisting of highly fractured granites, gneisses and schists from which rockfall with sizes up to several cubic meters are frequently triggered. The area is covered by an open forest stand (≤750 trees ha$^{-1}$) predominantly composed of Scots pine (*Pinus sylvestris*). The presence of fresh blocks scattered throughout the slope, frequent scars on the stem surface of trees (Fig. 3A) or decapitated trees clearly attest to the ongoing and strenuous rockfall activity at the study site. At the bottom of the talus slope, rockfall threatens a 1-km-long section of the international road E27 connecting Martigny to the Aosta Valley as well as the local Martigny-Orsières railway line (Fig. 2D).

### Rockfall hazard assessment

Several rockfall events have reached the main road or the railway line and were reported in cantonal archives. Yet, no historical catalogue of past rockfall activity is specifically available at our study site. As a consequence, we used (1) rockfall protection barriers and (2) tree-ring series as recorders of rockfall hazard.

#### Rockfall hazard assessment based on rocks deposited in rockfall protection barriers

The heavy traffic on the main road, both for the transport of persons and goods across Grand St. Bernard Pass, but also due to the large influx of tourists into *Val de Bagnes* (with the widely known resort of *Verbier*) results in dense car, bus, truck and train traffic which in turn exacerbates rockfall risk. As a consequence, since 1994, several protective countermeasures have been realized, including rockfall protection barriers (with a capacity of 2,000 kJ) and embankments (4 m in height) at the bottom of the slope (between 665 and 720 m asl; Fig. 2) to reduce rockfall risk on transportation networks. To estimate rockfall hazard at the level of these mitigation structures, we inventoried all rocks and boulders trapped in each of the structures. Given the
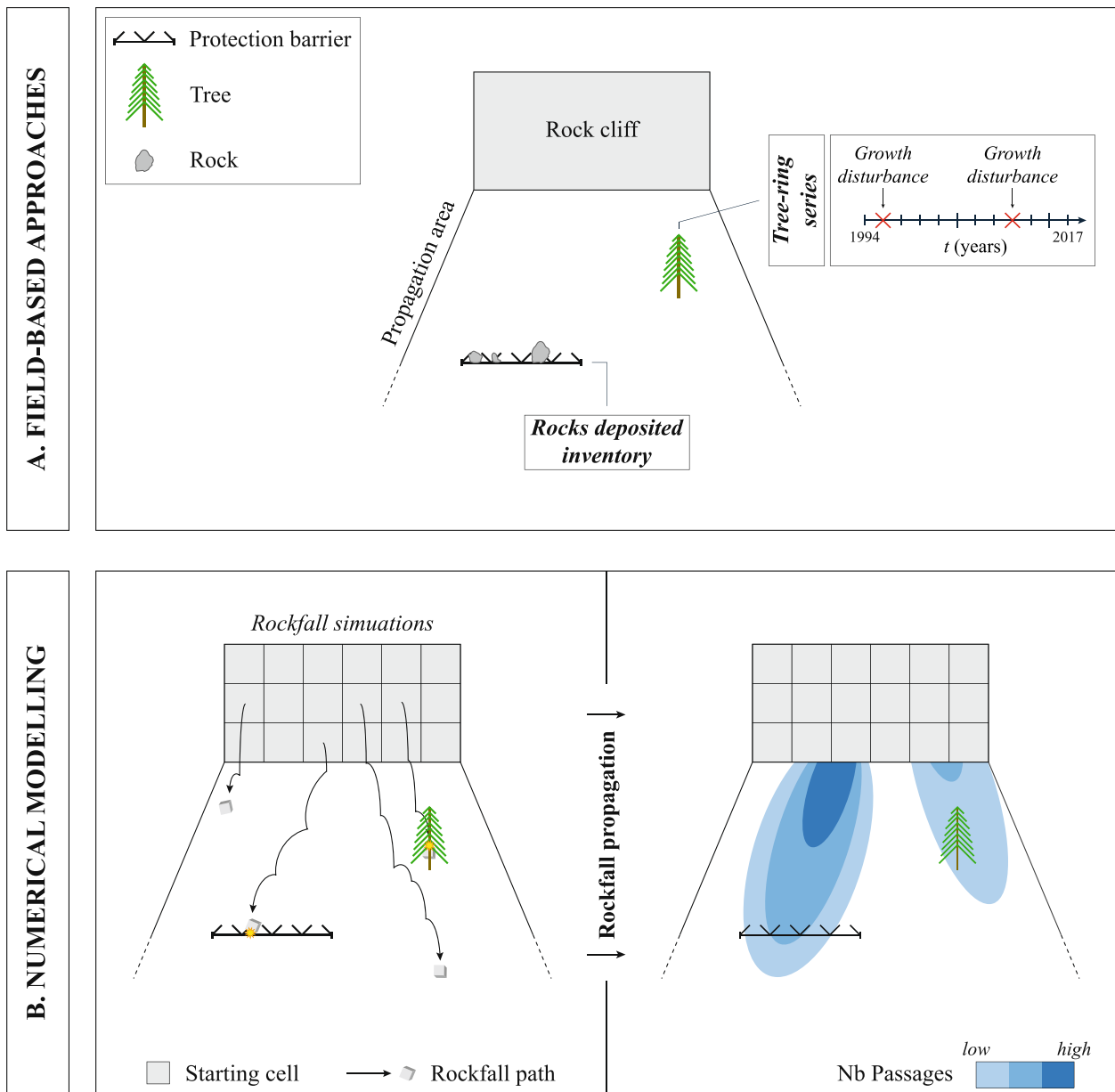
Protection barrier

Tree

Rock

Rock cliff

Propagation area

*Tree-ring series*

*Growth disturbance* *Growth disturbance*

1994 $t$ (years) 2017

*Rocks deposited inventory*

**B. NUMERICAL MODELLING**

*Rockfall simuations*

**Rockfall propagation**

Starting cell ⟶ Rockfall path

*low* *high*

Nb Passages

**Fig. 1** Schematic representation of the two-step procedure used to quantify rockfall release frequency ($\lambda$) at the cliff level: (**A**) we evaluated rockfall hazard values $H_z$ at various locations ($z$) on the slope, namely at the level of protection barriers and of each injured trees using the 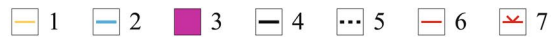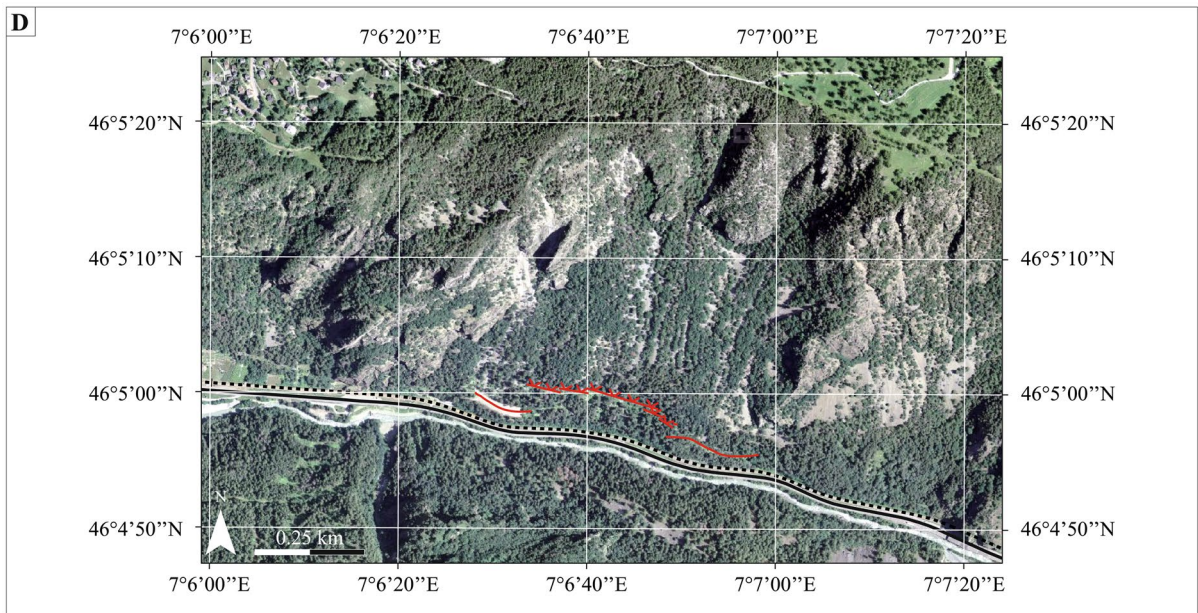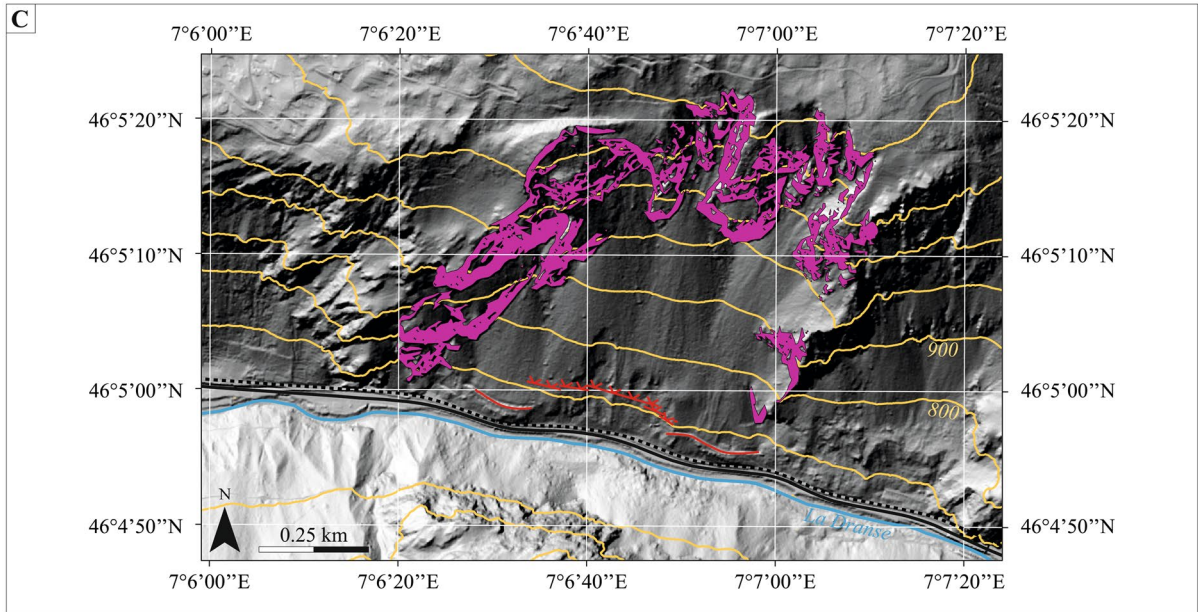number of 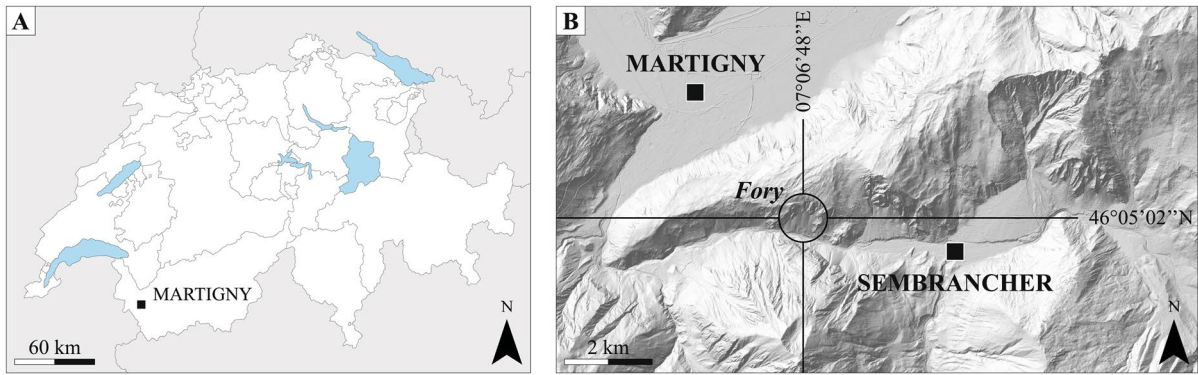rocks deposited in protection structures and growth disturbances in tree-ring series, respectively. These values were then (**B**) translated into rockfall release frequencies ($\lambda$) based on the numerical modeling of rockfall aimed at estimating reach probabilities ($p_z$) of individual rocks in the model.

parallelepiped shapes of rocks, we estimated volume based on the length of their x-, y- and z-axes. The rockfall hazard was thereafter computed as the ratio between the number of rocks deposited in mitigation structures and the number of years elapsed since their construction (as a mean hazard value given in events $yr^{-1}$). We considered all rocks deposited behind the protection barriers as they had not been removed since the initial installation of the defence structures. By contrast, we disregarded material left above the embankments because rockfall deposits have been removed periodically from these structures.

### Estimation of rockfall hazard using tree injuries

On forested slopes, the interaction of rocks with trees leaves dateable evidence of rockfall activity on the stem and in the growth-ring records of injured trees. Forests on rockfall slopes can therefore be seen as a natural archive of past events that can be explored with dendrogeomorphic techniques (Stoffel and Corona 2014).

In the field, we collected 250 increment cores from 66 Scots pine (*P. sylvestris L.*) trees distributed along two main rockfall corridors (C1 and C3; Fig. 4A) with a Pressler increment borer in summer 2018. One increment core (max. 40 × 0.5 cm) was taken at the lateral edges

of each visible scar (i.e. at the contact of the unaffected wood with the overgrowing callus tissue; Sachs 1991; Larson 1994; Schneuwly and Stoffel 2008). Increment cores (116 and 134 in rockfall paths C1 and C3, respectively) were then prepared and analyzed and data processed following standard dendrochronological procedures (Bräker 2002; Stoffel and Bollschweiler 2008). In the context of this study, the first layer of callus tissue within a tree ring was used to determine the (intra-) annual timing of past rockfall activity. To homogenize rockfall hazards computed from tree-ring series with data from protection barriers, we retained only those growth disturbances that occurred over the last 23 years, i.e. the period since the construction of rockfall defence infrastructure on the slope.

## Rockfall trajectory simulations

To estimate rockfall frequency out of the cliff compartment on the basis of the hazard values derived from deposits in barriers and scars on trees, a precise evaluation of the reach probability needs to be undertaken. Here, the latter has been obtained from an extensive dataset of 3D rockfall simulations.

### Numerical modeling of rockfall events

Rockfall was simulated on a digital elevation model (DEM; $2 \times 2$ m) with the probabilistic, process-based rockfall trajectory model Rockyfor3D (v5.0) (Dorren 2012). This model combines physically based, deterministic algorithms with stochastic approaches to simulate rockfall in three dimensions. Rockyfor3D calculates sequences of classical, uniformly accelerated parabolic free fall through the air and rebounds on the slope surface and trees (for details see Dorren et al. 2005). During each rebound, the model allows the block to deviate from its direction before rebounding. If an impact against a tree takes place, part of the rock energy is dissipated as a function of the stem diameter of the corresponding tree and the relative position between the rock and the tree's center.

In the transit area of rockfall (i.e. the zone located between the rockfall source and the depositional area), Rockyfor3D uses a tangential ($r_t$) and a normal ($r_n$) coefficient of restitution to calculate rock rebound on the slope surface (Volkwein et al. 2011). The tangential and the normal coefficient of restitution define the reduction in tangential velocity and the change in normal velocity during impact, respectively. Both coefficients depend on (*i*) rock shape and radius as well as on (*ii*) the depth of the impact crater during a rebound (Dorren et al. 2005). Given that the composition and size of the material covering the slope surface and $r_n$ values are closely related to land use, they were translated into several land-use and land-cover (LULC) classes.

In this study, the LULC map was derived from field observations and the analysis of aerial photographs before integration into Rockyfor3D. Soil types (e.g., fine soil material or bedrock) and roughness parameters were associated with each LULC class. For roughness, three variables were added to represent obstacle height encountered



**Fig. 3** View of (**A**) a multi-impacted pine stem (yellow dotted line) sampled at the vicinity of the cliff and (**B**) rockfall protection barriers installed in the lowest portion of the talus slope

on 10% (Rg10), 20% (Rg20) and 70% (Rg70) of the surface, respectively. In the upper part of the slope, at the vicinity of the cliff, the talus is mainly composed of small rock fragments and roughness values were set to 0.1 (Rg10), 0.35 (Rg20), and 0.20 m (Rg70). In the lower part of the slope, the scree is dominated by pluri-decimetric blocks and the model was therefore parametrized with values of 0.15, 0.15 and 0.25 m for Rg10, Rg20 and Rg70, respectively. The density of the forest stand, mean diameter of trees, and standard deviations thereof have been estimated from field observations.

Based on these values, the Rockyfor3D model randomly placed a given number of trees within each forested pixel (2 × 2m) of the slope. All settings are summarized in Table 1.

Mapping of potential release areas and rockfall reach probability
At the cliff, all cells (2 × 2m) with slope values >51° (42,925 cells) were considered potential rockfall release sources and mapped in a Geographical Information System (GIS). On the basis of the 2-m DEM resolution, the planar potential surface of the release area was
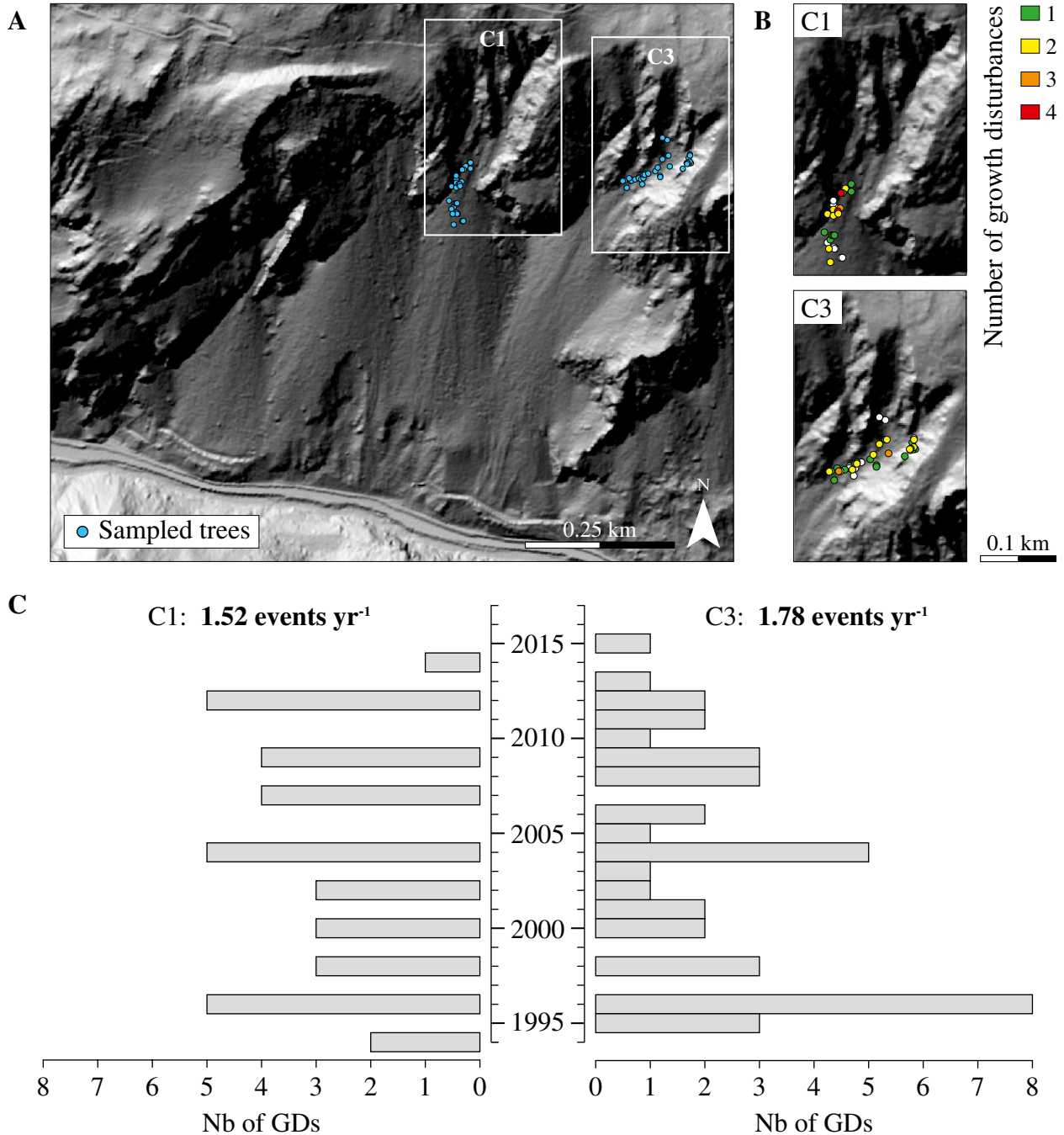


**Fig. 4** (**A**) Location of the trees sampled in rockfall plots C1 and C3. (**B**) Number of growth disturbances (GDs) dated in tree-ring series since 1994. (**C**) Annual number of GDs dated in tree-ring series over the period 1994-2017 in plots C1 and C3, respectively. Rockfall hazard values averaged 1.52 events yr⁻¹ in C1 and 1.78 events yr⁻¹ in C3

estimated to 17.2 hm$^2$. To estimate the real surface of the release area from the planar surface measured on the DEM, the following trigonometric correction was applied:

$$S = \sum_{i=1}^{n} \frac{x^2}{cos(\theta_i)} \quad (4)$$

where $x$ is the raster resolution and $\theta$ is the slope angle of release sources.

Based on Eq. (4), surface $S$ was estimated to 38 hm$^2$. Rock density in each source cell was set to 2,750 kg m$^{-3}$. In the transition area, the position of each sampled tree was recorded with a 1-m precision GPS device and placed in Rockyfor3D, while the row of rockfall protection barriers was considered as a continuous line.

A total of 1600 rockfall events with volumes randomly extracted between 0.5 and 2.5 m$^3$ were simulated with Rockyfor3D from each of the 42,925 potential source cells, resulting in a total of 68,680,000 simulated rockfall trajectories. Based on observations, $v=0.5$ m$^3$ was defined as the minimum block volume that can significantly damage pine trees at the study site, while the upper limit ($v=2.5$ m$^3$) corresponds to the largest block observed on the slope. Given the diameters of (*i*) the sampled trees (60 cm on average), (*ii*) the falling blocks (1-1.7m) and (*iii*) the resolution of the DEM (2×2m), we consider that each block reaching a raster cell containing a sampled tree will likely cause damage to its stem. For each simulation resulting in an impact with a sampled tree or the protection barrier, we systematically recorded simulation and object IDs and, most importantly, on the starting cell of rockfall. This database was then used to evaluate the rockfall reach probability $p$ at the level of the rockfall protection barrier and of each sampled tree, as:

$$p_z = \frac{Sim_z}{Sim_{Tot}} \quad (5)$$

where $Sim_z$ is the total number of simulations reaching $z$, i.e., the protection barriers and sampled trees, and $Sim_{Tot}$ is the total number of simulations.

## Results

### Rockfall hazard
Along the 420-m-long rockfall protection barriers, we inventoried a total of 24 blocks with volumes ranging from 0.06 m$^3$ to 2.45 m$^3$

in 2017. Among these events, only eight were larger than 0.5 m$^3$. Given the age of the mitigation structures—they were installed in 1994—rockfall hazard at the level of the barriers is estimated at 0.348 events yr$^{-1}$.

Similarly, 92 and 110 growth disturbances (GD) could be dated the in tree-ring series of *P. sylvestris* trees rockfall paths C1 and C3 between 1860-2017 and 1850-2017, respectively. For the period 1994-2017, for which we also have data from the rockfall barriers, 35 GD (in 19 out of 30 trees) and 41 GD (in 27 out of 36 trees) were retrieved from the tree-ring records (Fig. 4). Half of the trees sampled (50%) showed one GD during this period, 39% of the sampled trees had two GD. The maximum number of impacts between 1994 and 2017 observed in individual trees was 4 and 3 in paths C1 and C3, respectively. Based on the 19 and 27 trees that recorded, at least, one GD over the period 1994–2017, average rockfall hazard is equal to 1.52 events yr$^{-1}$ (C1) and 1.78 events yr$^{-1}$ (C3; Fig. 4C). At the level of individual trees, hazard values range from 0.043 to 0.174 events yr$^{-1}$.

### Reach probability

Regardless of the volume, 761,523 out of the 68,680,000 rocks simulated from the release surfaces reached the rockfall protection barriers, resulting in a reach probability $p_z$, of 0.011. Similarly, 2,162,530 and 2,486,751 impacts were recorded on trees sampled in plots C1 and C3, respectively, resulting in a rockfall reach probability equal to 0.031 and 0.036. Individual rockfall reach probabilities, computed as the ratio between the number of rocks impacting a sampled tree and the total number of simulations, therefore range between 0.0001 and 0.0049. At C1, reach probabilities are in the range 0.0008–0.004; they exceed 0.001 in the case of 15 out of the 27 trees sampled in C3.

### Rockfall release frequency

Coupling three-dimensional process models and hazard values retrieved from rockfall protection barriers and individual trees allowed quantification of rockfall release frequencies (as events yr$^{-1}$ hm$^{-2}$) at the level of the cliff. Based on the number of rocks deposited in protection

**Table 1** Values used for the parameterization of the Rockyfor3D model. Roughness is estimated with the Rg70, Rg20, and Rg10 values representing the height (in cm) of obstacles encountered by the falling block on 70%, 20% and 10% of the plot surface. The normal coefficient of restitution, $r_n$, defines the change in normal velocity after an impact and strongly depends on soil type. The density of the forest stand is expressed as a number of trees per hectare (Nb trees$^{-1}$ ha$^{-1}$). The mean diameter of trees and associated standard deviation are described as DBH mean and DBH std, respectively

| LULC type | Rg70 | Rg20 | Rg10 | $r_n$ | Nb trees$^{-1}$ ha$^{-1}$ | DBH Mean | DBH std |
|---|---|---|---|---|---|---|---|
| Cliff | 0 | 0 | 0.05 | 0.53 | 0 | 0 | 0 |
| Scree | 0.15 | 0.35 | 0.15 | 0.38 | 0 | 0 | 0 |
| Rockfall corridors | 0.10 | 0.35 | 0.20 | 0.38 | 750 | 30 | 10 |
| Densely forested area | 0.15 | 0.15 | 0.25 | 0.38 | 750 | 30 | 10 |
| Partially forested area | 0.15 | 0.15 | 0.25 | 0.33 | 500 | 30 | 10 |

barriers, we derived a release frequency of 0.82 events $yr^{-1} hm^{-2}$. In the case of the 46 impacted trees, we computed release frequency values for each tree in plots C1 and C3 individually (Fig. 5). Here, release frequency values ranged from 0.28 to 18 events $yr^{-1} hm^{-2}$. The average release frequency as obtained from impacted trees is 1.45 events $yr^{-1} hm^{-2}$ (standard deviation: 0.96) for C1 and 2.94 events $yr^{-1} hm^{-2}$ (standard deviation: 3.8) for C3. Despite the important differences between the two mean values derived for plots C1 and C3, the related probability density functions presented in Fig. 5A, B show comparable modal (1.35 and 0.99 events $yr^{-1} hm^{-2}$ for C1 and C3, respectively) and median values (1.3 and 1.5 events $yr^{-1} hm^{-2}$ for C1 and C3, respectively).

**Release surfaces**

Information on the starting cell IDs was stored in the Rockyfor3D database for each individual simulation landing in the rockfall

**Fig. 5** Probability density functions of rockfall release frequencies as obtained from the tree-ring series at plots C1 (**A**) and C3 (**B**). On average, release frequencies were 1.45 events $yr^{-1} hm^{-2}$ (C1) and 2.94 events $yr^{-1} hm^{-2}$ (C3). Modal and median values reached 1.35 and 1.3 events $yr^{-1} hm^{-2}$ for C1, they were 0.99 and 1.5 events $yr^{-1} hm^{-2}$ at C3
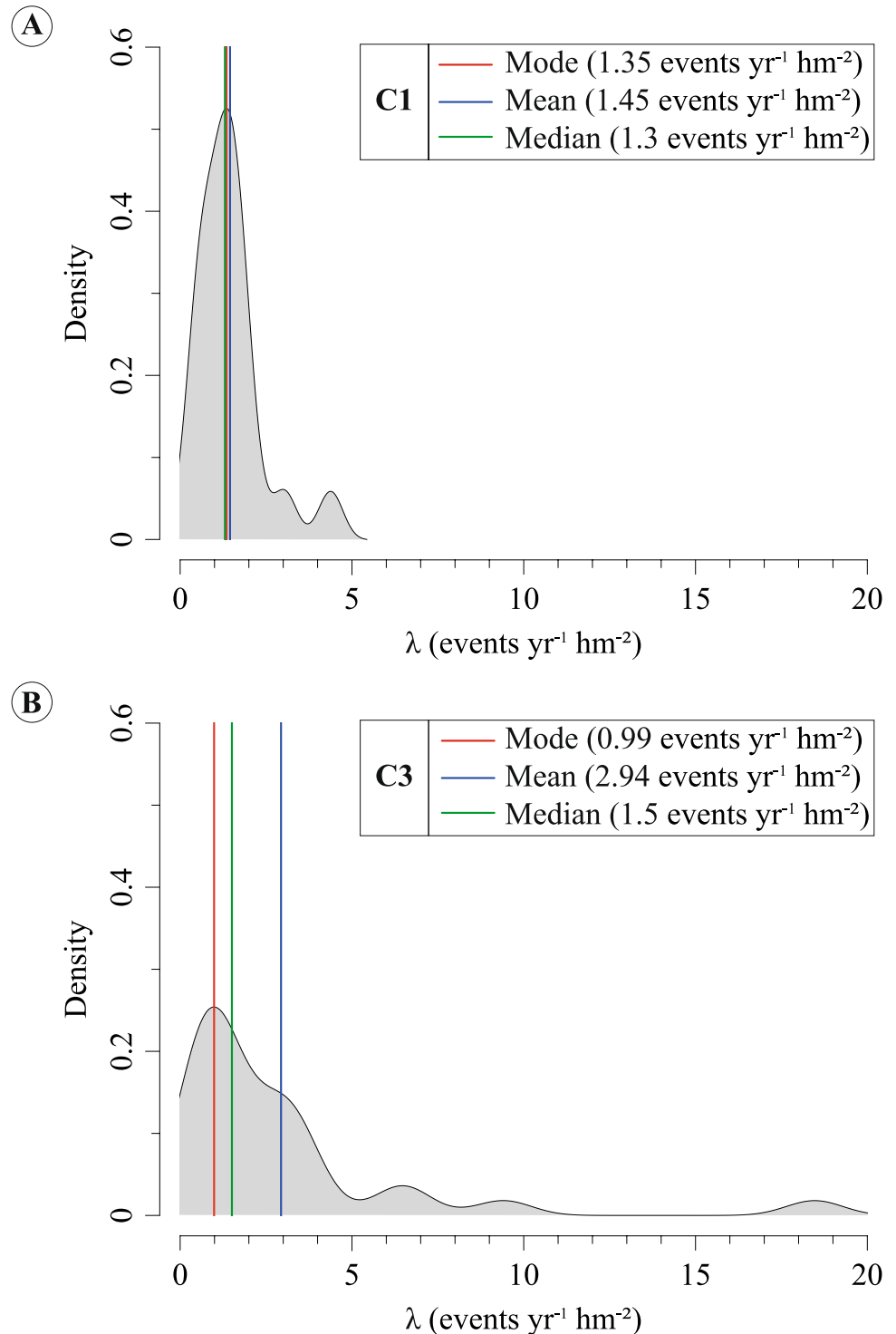
protection barriers or impacting sampled trees. Based on these records, we then delineated precisely those cliff areas that are susceptible to reach the mitigation structures and the impacted trees sampled in plots C1 and C3. The results presented in Figure 6 show three distinct release areas located in the northwestern, central, and northeastern portions of the La Fory cliff. The northwestern release area is at the origin of the rockfall deposits behind the protection barriers and is composed of 9,537 raster cells, with a total surface of 8.8 hm$^2$ (Fig. 6A). Therefore, a release frequency of 0.82 events yr$^{-1}$ hm$^{-2}$ can be attributed to this compartment. Similarly, 5,093 and 3,114 starting cells located in the central and northeastern portions of the cliff are susceptible to trigger rockfalls that cause damage to trees in plots C1 and C3, respectively. Given the resolution of the DEM ($2 \times 2$ m) and after trigonometric correction (Eq. (4)), the surfaces of the two rockfall release compartments are 4.1 (Fig. 6B) and 2.6 hm$^2$ (Fig. 6C). They are assigned a rockfall release frequency of 1.35 and 0.99 events yr$^{-1}$ hm$^{-2}$, respectively.

## Discussion

The design and optimization of structural and non-structural rockfall protection measures should be supported by a comprehensive risk analysis and evaluation (Volkwein et al. 2011) which in turn should rely on a detailed assessment of existing rockfall hazard. The latter necessarily includes an evaluation of (*i*) the temporal probability (in terms of frequency normalized to surface unit) and spatial susceptibility of rockfall, (*ii*) 3D trajectories, and (*iii*) rockfall intensity (in terms of energy) at each position along the path of a falling rock or boulder (Corominas and Moya 2008; Volkwein et al. 2011).

### Advantages of using tree-ring data, rockfall deposits and modeling approaches in combination

One major limitation of hazard analyses typically is the lack of information regarding the temporal probability and thus the representation of model output in terms of real frequencies (Ferrero et al. 2016). In practice, the estimation of rockfall frequency is the single most challenging aspect which existing approaches have not yet addressed specifically when it comes to the management of rockfall hazards. Indeed, the spatial and temporal heterogeneity of scarcely available rockfall inventories (Dussauge et al. 2003; Sass and Oberlechner 2012; Eckert et al. 2020) has so far precluded precise quantification of rockfall frequencies at decadal to centennial timescales. On the other hand, rather expensive but highly resolved data that are acquired from remote sensing (e.g., LiDAR and photogrammetry) and direct monitoring (e.g., crackmeters, extensometers, and survey prisms) can yield valuable insights into process dynamics in the short term, yet they are in most instances too much constrained—both in time and space (Westoby et al. 2018; Lato et al. 2015; Sättele et al. 2016; Kromer et al. 2017; Carlá et al. 2019)—to meet the requirements of long-term records in hazard approaches. Therefore, new methods are still critically needed to reconcile the dilemma between cost, accuracy and temporal coverage for an implementation at scales relevant for rockfall hazard assessment.
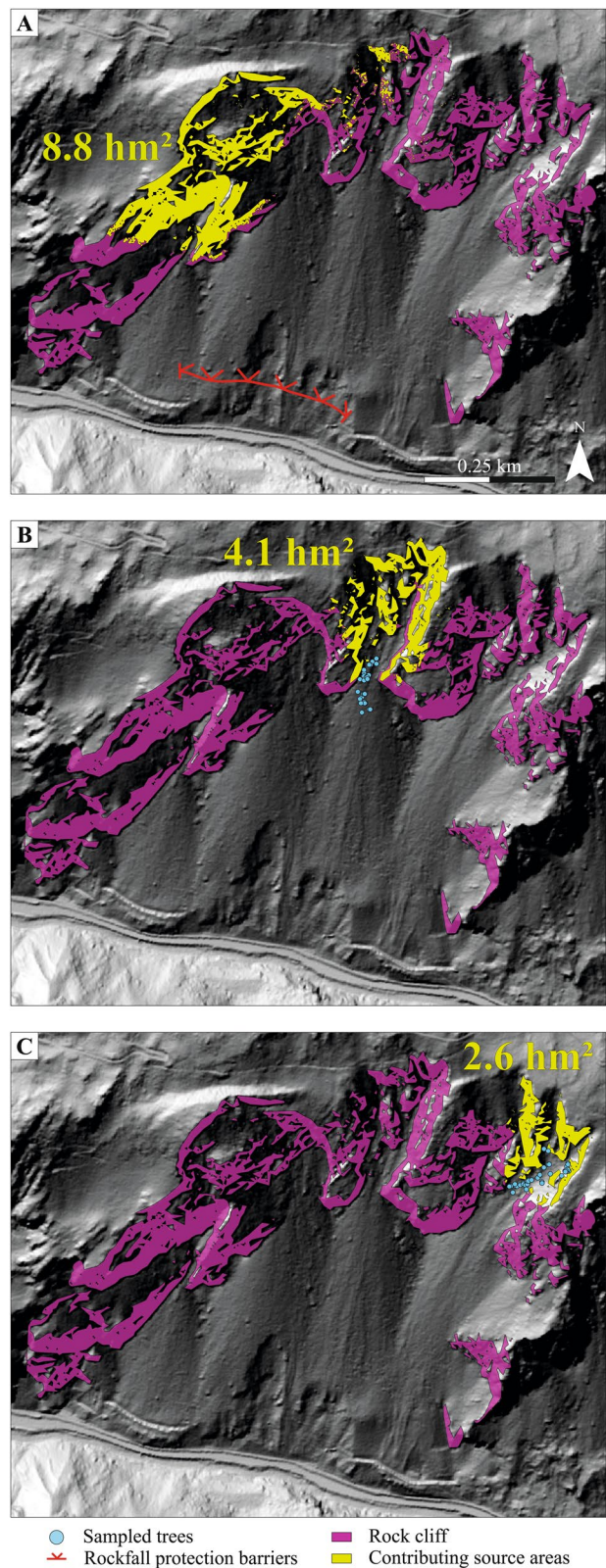


**Fig. 6** Cliff compartments (in yellow) threatening the rockfall protection barriers (**A**) as well as plots C1 (**B**) and C3 (**C**). The northwestern portion of the La Fory cliff sends rockfall to the protection barriers and has a total surface of 8.8 hm$^2$ (**A**). The central (**B**) and northeastern (**C**) compartments are susceptible to cause damage to plots C1 and C3 have surfaces of 4.1 (C1) and 2.6 hm$^2$ (C3), respectively

In this study, we developed an approach that couples records on past rockfall activity retrieved from protection barriers and tree-ring analysis with rockfall modeling, with the final aim to quantify release frequencies at the level of a cliff. At the study site of La Fory, we used a total of 76 GDs recorded in tree-ring series and 8 rocks >0.5 m$^3$ deposited in mitigation structures between 1994 and 2017 to quantify rockfall hazard values at the site. These values, ranging from 0.348 to 1.78 events yr$^{-1}$, were then translated into rockfall release frequencies with the help of simulation results. In that sense, reach probabilities were estimated from 68,680,000 rockfall trajectories to derive rockfall release frequencies of 0.82 events yr$^{-1}$ hm$^{-2}$ for the protection barriers as well as 1.35 and 0.99 events yr$^{-1}$ hm$^{-2}$ for two tree plots (C1 and C3) located at the vicinity of the cliff.

Based on the results, we can state that our approach coupling process modeling with field-based evidence indeed represents a promising alternative to quantify the temporal probability of rockfall failure at sites for which rockfall inventories are not available or poorly reliable. As such, this new approach should be of major relevance for hazard management as it allows to (*i*) translate rockfall activity estimated at virtually any location on the slope into rockfall frequencies for compartments of the cliff, (*ii*) provide estimates of rockfall in space and time (in the present case for 8.8, 4.1 and 2.6 hm$^2$ and over several decades) that are usually compatible with stakeholder constraints and (*iii*) that can be included in modeling efforts which in turn are ultimately leading to precise hazard maps and robust quantitative risk analyses (QRA). The latter, through their holistic character, will differ from previous studies in rockfall-prone environments as assessments have been restricted strictly to critical release areas (Corominas et al. 2005; Agliardi et al. 2009).

### Reliability and caveats of the new procedure

In the literature available for alpine regions (see Table 2 for a complete review), rockfall release frequencies have been quantified with different approaches (i.e., historical archives or LiDAR data in the majority of cases), periods (from a few years up to a century) and lithologies (most often in limestone). Due to the heterogeneity of existing studies, comparison between different approaches seems difficult. Yet,

the convergence between the rockfall frequencies obtained from the tree-ring records and data on the deposits left behind the protection barriers—that is from two completely independent datasets—pleads for the reliability and robustness of our results.

Despite these promising results, we should address several remaining limitations inherent to the newly developed approach here. From a perspective of hazard management, one remaining caveat is related to the fact that our procedure does not allow—unlike remote sensing approaches—to retrieve data on the distribution of volumes of released rocks from the cliff. This shortfall could, however, be overcome by a systematic mapping of fresh rockfall deposits on the slope under investigation (Farvacque et al. 2019). Furthermore, one could speculate that an overestimation of rockfall release frequencies could occur as a result of the (*i*) fragmentation of released blocks during ground contacts Giacomini et al. (2009); Wang and Tonon (2011); Corominas et al. (2019), which in turn could cause a dispersion of trajectories and subsequent impacts on trees along the falling path (Corona et al. 2017) as well as a higher number but smaller volume of rocks deposited in the nets (Trappmann and Stoffel 2013; Trappmann et al. 2014; *ii*) secondary remobilization of previously failed material (that was stored temporarily on the slope) by earth-surface processes (Krautblatter and Dikau 2007) such as other falling rock masses, debris flows or snow avalanches (Borella et al. 2019); or the (*iii*) occurrence of multiple scars during the same year on several stems that were, in reality, inflicted by a single rock (Trappmann et al. 2014). By contrast, a bias could be inherent to the spatio-temporal probability of rockfall failure should the threshold of critical slope angle for the detection of potential release sources have been underestimation. Similarly, the dendrogeomorphic reconstruction proposed here will probably only partly reflect rockfall activity as a result of (*i*) the spatial distribution and the limited number of sampled trees, which will prevent interception of all rockfall trajectories that have occurred in the past; and (*ii*) old and completely healed injuries that are sometimes difficult to be detected in tree-ring series (Trappmann and Stoffel 2013), even more so in pine trees (Stoffel et al. 2006). In future studies, these limitations could be overcome by using optimized sample strategies aimed at estimating missed rockfall events from dendrogeomorphic time series (Mainieri 2020; Mainieri et al. 2020a; b).

**Table 2** Rockfall release frequencies ($\lambda$, in events yr$^{-1}$ hm$^{-2}$) available from existing literature in the Alps. T represents the period covered by observations (in years) and S$_C$ the surface of the cliff (in hm$^2$) used to compute $\lambda$

| References | Site | Geological setting | Technique | T | S$_C$ | Volumes | $\lambda$ |
|---|---|---|---|---|---|---|---|
| Dussauge-Peisser et al. (2002) | Grenoble | Calcareous | Historical archives | 60 | 2 10$^{-2}$ | >50 m$^C$ | 0.002 |
| Dussauge-Peisser et al. (2002) | Arly Gorges | Metamorphic rocks | Historical archives | 22 | 55 | >20 m$^2$ | 0.15 |
| Guerin et al. (2014) | Mont St-Eynard | Limestone | LiDAR | 3.2 | 15 | >1 m$^\lambda$ | 0.85 |
| D'Amato et al. (2015) | Gorgette | Limestone | LiDAR | 3.2 | 5 | >1 m$^C$ | 0.96 |
| D'Amato et al. (2015) | Venosc | Gneiss | LiDAR | 3.2 | 37 | >1 m$^\lambda$ | 0.085 |
| Hantz et al. (2016) | Haute-Savoie | Limestone | Unknown | 22 | 8 10$^3$ | >1 m$^3$ | 0.002 |
| Hantz et al. (2016) | Isére | Limestone | Unknown | 62 | 6 10$^3$ | >1 m$^3$ | 0.001 |
| Farvacque et al. (2019) | Crolles | Limestone | Field inventories | 100 | 128 | >1 m$^3$ | 0.015 |

## Conclusions

The combination of rockfall inventories using deposits found in protection barriers, growth disturbances detected in tree-ring series as well as the 3D, physically based modeling of rockfall has been used, for the first time, to quantify the spatio-temporal probability of rockfall failure for a cliff in the Swiss Alps. Field-based approaches allowed determination of hazard values for different segments across the slope, whereas the modeling enabled a translation of the hazard values into rockfall frequencies at the scale of individual cliff compartments. Results derived from the dendrogeomorphic approach and rockfall inventories, ranging between 0.8 and 1.4 events $yr^{-1} hm^{-2}$, are in good agreement and support each other. Although the approach may potentially suffer from possible caveats—in particular the lack of a rockfall volume distribution—we conclude that the release frequencies derived from this reproducible and cost effective approach can be used in the future to establish hazard and risk maps that will enable prioritization and the dimensioning of protection measures. Considering its significant contribution, namely to quantify rockfall release frequencies, we recommend that this new procedure should be included whenever possible in risk management strategies in rockfall-prone areas, as it can substantially enhance hazard assessments at limited additional cost.

## References

Agliardi F, Crosta G (2003) High resolution three-dimensional numerical modelling of rockfalls. Int J Rock Mech Min Sci 40(4):455–471

Agliardi F, Crosta GB, Frattini P (2009) Integrating rockfall risk assessment and countermeasure design by 3d modelling techniques. Natural Hazards and Earth System Science 9(4):1059–1073

Asteriou P, Saroglou H, Tsiambaos G (2013) Rockfalls: influence of rock hardness on the trajectory of falling rock blocks. Bulletin of the Geological Society of Greece 47(4):1684

Benjamin J, Rosser NJ, Brain MJ (2020) Emergent characteristics of rockfall inventories captured at a regional scale. Earth Surf Proc Land 45(12):2773–2787

Bourrier F, Dorren L, Nicot F, Berger F, Darve F (2009) Toward objective rockfall trajectory simulation using a stochastic impact model. Geomorphology 110(3–4):68–79

Bourrier F, Hungr O (2013) Rockfall Dynamics: A Critical Review of Collision and Rebound Models. In: Lambert S, Nicot F (eds) Rockfall Engineering. John Wiley & Sons Inc, Hoboken, NJ, USA, pp 175–209

Borella J, Quigley M, Krauss Z, Lincoln K, Attanayake J, Stamp L, Lanman H, Levine S, Hampton S, Gravley D (2019) Geologic and geomorphic controls on rockfall hazard: how well do past rockfalls predict future distributions? Natural Hazards and Earth System Sciences 19(10):2249–2280

Bräker OU (2002) Measuring and data processing in tree-ring research - a methodological introduction. Dendrochronologia 20(1–2):216

Budetta P, De Luca C, Nappi M (2016) Quantitative rockfall risk assessment for an important road by means of the rockfall risk management (ro.ma.) method. Bull Eng Geol Env 75(4):1377–1397

Carlà T, Nolesini T, Solari L, Rivolta C, Dei Cas L, Casagli N, (2019) Rockfall forecasting and risk management along a major transportation corridor in the Alps through ground-based radar interferometry. Landslides 16(8):1425–1435

Corominas J, Copons R, Moya J, Vilaplana JM, Altimir J, Amigó J (2005) Quantitative assessment of the residual risk in a rockfall protected area. Landslides 2(4):343–357

Corominas J, Moya J (2008) A review of assessing landslide frequency for hazard zoning purposes. Eng Geol 102(3–4):193–213

Corominas J, Matas G, Ruiz-Carulla R (2019) Quantitative analysis of risk from fragmental rockfalls. Landslides 16(1):5–21

Corona C, Lopez-Saez J, Favillier A, Mainieri R, Eckert N, Trappmann D, Stoffel M, Bourrier F, Berger F (2017) Modeling rockfall frequency and bounce height from three-dimensional simulation process models and growth disturbances in submontane broadleaved trees. Geomorphology 281:66–77

Crosta GB, Agliardi F (2003) A methodology for physically based rockfall hazard assessment. Natural Hazards and Earth System Science 3(5):407–422

D'Amato J, Guerin A, Hantz D, Rossetti J-P, Jaboyedoff M (2015) Investigating Rock Fall Frequency and Failure Configurations Using Terrestrial Laser Scanner. In: Lollino G, Giordan D, Crosta GB, Corominas J, Azzam R, Wasowski J, Sciarra N (eds) Engineering Geology for Society and Territory -, vol 2. Springer International Publishing, Cham, pp 1919–1923

D'Amato J, Hantz D, Guerin A, Jaboyedoff M, Baillet L, Mariscal A (2016) Influence of meteorological factors on rockfall occurrence in a middle mountain limestone cliff. Nat Hazard 16(3):719–735

Dorren L (2012) Rockyfor3d (v5.1) revealed – Transparent description of the complete 3d rockfall model. ecorisQ paper 32

Dorren LK, Berger F, le Hir C, Mermin E, Tardif P (2005) Mechanisms, effects and management implications of rockfall in forests. For Ecol Manage 215(1–3):183–195

Dussauge C, Grasso J-R, Helmstetter A (2003) Statistical analysis of rockfall volume distributions: Implications for rockfall dynamics: Rockfall volume statistics. J Geophys Res Solid Earth 108:B6

Dussauge-Peisser C, Helmstetter A, Grasso JR, Hantz D, Desvarreux P, Jeannin M, Giraud A (2002) Probabilistic approach to rock fall hazard assessment: potential of historical data analysis. Natural Hazards and Earth System Science 2(1–2):15–26

Eckert N, Mainieri R, Bourrier F, Giacona F, Corona C, Le Bidan V, Lescurier A (2020) Une base de données événementielle du risque rocheux dans les alpes françaises. Revue Francaise de Geotechnique 163:3

Farvacque M, Lopez-Saez J, Corona C, Toe D, Bourrier F, Eckert N (2019) Quantitative risk assessment in a rockfall-prone area: the case study of the Crolles municipality (Massif de la Chartreuse, French Alps). Géomorphologie?: Relief, Processus, Environnement 25(1):7–19

Feng L, Intrieri E, Pazzi V, Gigli G, Tucci G (2020) A framework for temporal and spatial rockfall early warning using micro-seismic monitoring. Landslides

Ferrari F, Giacomini A, Thoeni K (2016) Qualitative Rockfall Hazard Assessment: A Comprehensive Review of Current Practices. Rock Mech Rock Eng 49(7):2865–2922

Ferrero A, Umili G, Vagnon F (2016) Analysis of discontinuity data obtained with remote sensing tools to generate input for EC7 design. In: Mechanics Rock, Engineering Rock (eds) From the Past to the Future (Cappadocia. CRC Press, Turkey, pp 1115–1119

Ferrero AM, Migliazza MR, Pirulli M, Umili G (2016) Some Open Issues on Rockfall Hazard Analysis in Fractured Rock Mass: Problems and Prospects. Rock Mech Rock Eng 49(9):3615–3629

Gallach X, Ravanel L, Egli M, Brandova D, Schaepman M, Christl M, Gruber S, Deline P, Carcaillet J, Pallandre F (2018) Timing of rockfalls in the Mont Blanc massif (Western Alps): evidence from surface exposure dating with cosmogenic 10Be. Landslides 15(10):1991–2000

Giacomini A, Buzzi O, Renard B, Giani G (2009) Experimental studies on fragmentation of rock falls on impact with rock surfaces. International Journal of Rock Mechanics and Mining Sciences 46(4):708–715

Giani GP, Giacomini A, Migliazza M, Segalini A (2004) Experimental and Theoretical Studies to Improve Rock Fall Analysis and Protection Work Design. Rock Mech Rock Eng 37(5):369–389

Guerin A, Hantz D, Rossetti J-P, Jaboyedoff M (2014) Brief communication "Estimating rockfall frequency in a mountain limestone cliff using terrestrial laser scanne". Natural Hazards and Earth System Sciences Discussions 2(1):123–135

Guerin A, Stock GM, Radue MJ, Jaboyedoff M, Collins BD, Matasci B, Avdievitch N, Derron M-H (2020) Quantifying 40 years of rockfall activity in Yosemite Valley with historical Structure-from-Motion photogrammetry and terrestrial laser scanning. Geomorphology 356:107069

Hantz D, Dewez T, Levy C, Guerin A, Jaboyedoff M (2016) Rockfall frequency in different geomorphological conditions. 3rd RSS Rock Slope Stability conference, Lyon

Hungr O, Leroueil S, Picarelli L (2014) The varnes classification of landslide types, an update. Landslides 11(2):167–194

Kanari M, Katz O, Weinberger R, Porat N, Marco S (2019) Evaluating earthquake-induced rockfall hazard near the Dead Sea Transform. Nat Hazard 19(4):889–906

Krautblatter M, Dikau R (2007) Towards a uniform concept for the comparison and extrapolation of rockwall retreat and rockfall supply. Geografiska Annaler: Series A, Physical Geography 89(1):21–40

Kromer R, Lato M, Hutchinson DJ, Gauthier D, Edwards T (2017) Managing rockfall risk through baseline monitoring of precursors using a terrestrial laser scanner. Can Geotech J 54(7):953–967

Lambert S (Ed.) (2011) Rockfall engineering. ISTE, London. OCLC: 774358397

Larson PR (1994) The Vascular Cambium: Development and Structure. Springer Science & Business Media Ed

Lato MJ, Gauthier D, Hutchinson DJ (2015) Rock Slopes Asset Management: Selecting the Optimal Three-Dimensional Remote Sensing Technology. Transportation Research Record: Journal of the Transportation Research Board 2510(1):7–14

Macciotta R, Martin CD, Cruden DM (2015) Probabilistic estimation of rockfall height and kinetic energy based on a three-dimensional trajectory model and Monte Carlo simulation. Landslides 12(4):757–772

Mainieri R (2020) La forêt, un intégrateur robuste de l'évolution de la dynamique des chutes de blocs dans un contexte de changements environnementaux? PhD thesis, COMMUNAUTÉ UNIVERSITÉ GRENOBLE ALPES, Grenoble Alpes

Mainieri R, Corona C, Chartoire J, Eckert N, Lopez-Saez J, Stoffel M, Bourrier F (2020a) Dating of rockfall damage in trees yields insights into meteorological triggers of process activity in the French Alps. Earth Surface Processes and Landforms

Mainieri R, Corona C, Lopez-Saez J, Stoffel M, Toe D, Dupire S, Eckert N, Bourrier F (2020b) Improved tree-ring sampling strategy enhances the detection of key meteorological drivers of rockfall activity. In press. Catena

Matasci B, Stock GM, Jaboyedoff M, Carrea D, Collins BD, Guérin A, Matasci G, Ravanel L (2018) Assessing rockfall susceptibility in steep and overhanging slopes using three-dimensional analysis of failure mechanisms. Landslides 15(5):859–878

Sachs T (1991) Pattern Formation in Plant Tissues, 1 ed. Cambridge University Press

Sass O, Oberlechner M (2012) Is climate change causing increased rockfall frequency in Austria? Natural Hazards and Earth System Science 12(11):3209–3216

Sättele M, Krautblatter M, Bründl M, Straub D (2016) Forecasting rock slope failure: how reliable and effective are warning systems? Landslides 13(4):737–750

Schneuwly D, Stoffel M (2008) Spatial analysis of rockfall activity, bounce heights and geomorphic changes over the last 50 years - A case study using dendrogeomorphology. Geomorphology 102(3–4):522–531

Stevens WD (1998) Rocfall: A tool for probablistic analysis, design of remedial measures and prediction of rockfalls. A thesis submitted in conformity with the requirements for the degree of Master of Applied Science, Graduate Department of Civil Engineering, University of Toronto

Stoffel M, Bollschweiler M (2008) Tree-ring analysis in natural hazards research&ndash; an overview. Nat Hazard 8(2):187–202

Stoffel M, Corona C (2014) Dendroecological Dating of Geomorphic Disturbance in Trees. Tree-Ring Research 70(1):3–20

Strunden J, Ehlers TA, Brehm D, Nettesheim M (2015) Spatial and temporal variations in rockfall determined from TLS measurements in a deglaciated valley, Switzerland: Rockfall in a deglaciated valley. J Geophys Res Earth Surf 120(7):1251–1273

Stoffel M, Wehrli A, Kühne R, Dorren LK, Perret S, Kienholz H (2006) Assessing the protective effect of mountain forests against rockfall using a 3d simulation model. Forest Ecology and Management 225(1–3):113–122

Trappmann D, Stoffel M (2013) Counting scars on tree stems to assess rockfall hazards: A low effort approach, but how reliable? Geomorphology 180–181:180–186

Trappmann D, Stoffel M, Corona C (2014) Achieving a more realistic assessment of rockfall hazards by coupling three-dimensional process models and field-based tree-ring data. Earth Surface Processes and Landforms 39(14):1866–1875

Umili G, Bonetto SMR, Mosca P, Vagnon F, Ferrero AM (2020) In Situ Block Size Distribution Aimed at the Choice of the Design Block for Rockfall Barriers Design: A Case Study along Gardesana Road. Geosciences 10(6):223

Varnes DJ (1984) Landslide hazard zonation: a review of principles and practice. No. 3 in Natural hazards. Unesco, Paris

Volkwein A, Schellenberg K, Labiouse V, Agliardi F, Berger F, Bourrier F, Dorren LKA, Gerber W, Jaboyedoff M (2011) Rockfall characterisation and structural protection – a review. Natural Hazards and Earth System Science 11(9):2617–2651

Wang Y, Tonon F (2011) Discrete Element Modeling of Rock Fragmentation upon Impact in Rock Fall Analysis. Rock Mechanics and Rock Engineering 44(1):23–35

Wang X, Frattini P, Crosta GB, Zhang L, Agliardi F, Lari S, Yang Z (2014) Uncertainty assessment in quantitative rockfall risk assessment. Landslides 11(4):711–722

Westoby MJ, Lim M, Hogg M, Pound MJ, Dunlop L, Woodward J (2018) Cost-effective erosion monitoring of coastal cliffs. Coast Eng 138:152–164

Zimmer VL, Sitar N (2015) Detection and location of rock falls using seismic and infrasound sensors. Eng Geol 193:49–60

**Manon Farvacque · Robin Mainieri · Franck Bourrier · Nicolas Eckert**

Université Grenoble Alpes, INRAE, UR ETNA, 2 rue de la papeterie, 38402 St-Martin-d'Hères, France
Email: manon.farvacque@unige.ch

**Manon Farvacque (✉) · Christophe Corona · Jérôme Lopez-Saez Markus Stoffel**

Climate Change Impacts and Risks in the Anthropocene, Institute for Environmental Sciences, University of Geneva - Bd, Carl-Vogt 66, CH-1205, Geneva, Switzerland
Email: manon.farvacque@unige.ch

**Christophe Corona**

Université Clermont Auvergne, CNRS GEOLAB UMR - 4 rue Ledru, 63057 Clermont-Ferrand, France

**Markus Stoffel**

Department of Earth Sciences, University of Geneva, rue des Maraîchers 13, CH-1205, Geneva, Switzerland

**Markus Stoffel**

Department F.-A. Forel for Environmental and Aquatic Sciences, University of Geneva - Bd, Carl-Vogt 66, CH-1205, Geneva, Switzerland

**David Toe**

Université Grenoble Alpes, INRAE, UR LESSEM - 2 rue de la papeterie, 38402 St-Martin-d'Hères, France